Author Manuscript

Author Manuscript

Author Manuscript

Author Manuscript

HHS Public Access

Author manuscript

IEEE Trans Biomed Circuits Syst. Author manuscript; available in PMC 2018 April 01.

Published in final edited form as:

IEEE Trans Biomed Circuits Syst. 2017 April ; 11(2): 336–346. doi:10.1109/TBCAS.2016.2620805.

Design and Testing of a Transcutaneous RF Recharging System for a Fetal Micropacemaker

Adriana N. Vest,
University of Southern California, Los Angeles, CA 90089 USA. She is now with the Department of Biomedical Engineering, Georgia Institute of Technology, Atlanta, GA 30332 USA

Li Zhou [Member, IEEE],
Department of Biomedical Engineering, University of Southern California, Los Angeles, CA 90089 USA

Xuechen Huang,
Department of Biomedical Engineering, University of Southern California, Los Angeles, CA 90089 USA

Viktoria Norekyan,
Department of Biomedical Engineering, University of Southern California, Los Angeles, CA 90089 USA

Yaniv Bar-Cohen,
Division of Cardiology, Children's Hospital Los Angeles; and USC Keck School of Medicine, Los Angeles, CA 90027 USA

Ramen H. Chmait, and
Department of Obstetrics and Gynecology, Keck School of Medicine, University of Southern California, Los Angeles, CA 90033 USA

Gerald Eli Loeb [Senior Member, IEEE]
Department of Biomedical Engineering, University of Southern California, Los Angeles, CA 90089 USA

Abstract

We have developed a rechargeable fetal micropacemaker in order to treat severe fetal bradycardia with comorbid hydrops fetalis. The necessarily small form factor of the device, small patient population, and fetal anatomy put unique constraints on the design of the recharging system. To overcome these constraints, a custom high power field generator was built and the recharging process was controlled by utilizing pacing rate as a measure of battery state, a feature of the relaxation oscillator used to generate stimuli. The design and *in vitro* and *in vivo* verification of the recharging system is presented here, showing successful generation of recharging current in a fetal lamb model.

Index Terms

Inductive recharging; pacemakers

Author Manuscript Author Manuscript Author Manuscript Author Manuscript

I. Introduction

We have developed a fetal micropacemaker to treat progressive complete heart block with comorbid hydrops in the human fetus. This rare condition occurs in several hundred pregnancies per year in the United States, but is life-threatening; once hydrops develops as a result of heart block, fetal demise is nearly inevitable if the fetus cannot be delivered due to prematurity or other clinical concerns [1–5]. Implanting our fetal micropacemaker could reverse the course of this condition, resulting in the resolution of hydrops within one to two weeks by pacing the heart and restoring adequate blood flow to the fetus. The fetus could then proceed with an otherwise normal gestation and delivery. Once born, the infant would be implanted with a standard adult pacemaker and epicardial lead, the standard of care for newborns with symptomatic bradycardia.

Several groups have attempted to pace these fetal patients in the past, but have been unsuccessful, likely due to complications from open surgery, lead placement or entanglement issues, and/or lead dislodgement due to fetal movement [6–10]. To overcome these failure modes, a successful fetal micropacemaker implantation must be performed with a minimally invasive technique in order to reduce the chance of surgical complications, and the device must be implanted entirely within the fetal chest, avoiding the complications associated with a trans-uterine lead.

Our device design overcomes the shortcomings of previous attempts and addresses the aforementioned requirements of fetal pacing by being implanted via a percutaneous approach through a standard fetal surgical cannula and with a form factor that can fit entirely in the chest wall (Fig. 1)[11]. The fetal instrumentation necessitates a cylindrical form that fits through the inside diameter of a 3.8 mm cannula. The potential market size of a mere 500 devices a year further constrains its engineering; the technology must be simple and inexpensive both to develop and to build.

We employ a simple relaxation oscillator based on a single transistor (PUT, Fig. 2), which uses only 7 components and keeps the pulse generator small while also meeting requirements for low power consumption and low development cost. Output capacitor C_{OUT} is charged through resistor R_C until its voltage reaches the threshold set by the programmable unijunction transistor (PUT) and biasing resistors R_1 and R_2. The PUT then switches to a low impedance state that allows the charge accumulated on C_{OUT} to discharge through the electrode and tissue, represented here as a capacitor in series with a resistor (C_{TISSUE} and R_{TISSUE}). The charge of the output pulse is equal to the charge accumulated on C_{OUT} and is fixed by the capacitance C_{OUT}, bias resistors R_1 and R_2, and supply voltage according to

$$Pulse\ Charge = C_{OUT} * V_{SUPPLY} \frac{R_2}{R_1 + R_2}\ \text{Coulombs} \quad (1)$$

Normal physiological changes in tissue impedance have a negligible effect on the stimulus duration or stimulus charge. Once C_{OUT} completely discharges, the PUT switches back into

Author Manuscript Author Manuscript Author Manuscript Author Manuscript

a high impedance state and begins another charge/discharge cycle at a period set by the time-constant R_C*C_{OUT}.

The rate of the oscillator is set to about 100 – 110 beats per minute (bpm) in order to provide an adequate heart rate to the distressed fetus, essentially functioning in fixed-rate pacing mode VOO. (Pacemaker code VOO stands for Ventricular pacing, no sensing (O), and no response to sensing (O) [12].) However, the rate also varies to a lesser degree according to the supply voltage. As the charge on the lithium ion cell (hereafter refered to as the lithium cell, or simply the cell) is drained, its voltage decreases, resulting in a small but detectable change in the rate of output pulses as the internal voltage drop in the transistor becomes a larger fraction of the supply voltage to the circuit. This relationship is calibrated during manufacturing of each micropacemaker (Fig. 3), and used to determine the state of the lithium cell, and therefore when to recharge. This technique was used to decide when to replace the earliest cardiac pacemakers circa 1960, which were based on a relaxation oscillator circuit similar to what we have used in this device. As voltage on the cell drops and recharging is not initiated, this particular relaxation oscillator design will drop its frequency until it ceases oscillation. When the pacemaker is recharged, oscillations begin again according to the calibration curve. This pacemaker is effective at treating bradycardia when it is pacing at a frequency of about 60 bpm, and it is delivering charge above the stimulation threshold for the cardiac tissue in which it is implanted [13]. Therefore, a lower operational limit will vary from patient to patient.

For power, the oscillator uses a tiny cylindrical lithium cell (Fig. 2, V_{CELL}, QL0003I Zero-Volt, Quallion). Devices with implanted lithium cells must conform to the IEC 62133 standard, which requires safety features that limit catastrophic mechanical and electrical failures. The cell chosen for this application is rated for human use and has a capacity of 3 mAh, which can sustain a typical stimulus output pulse of 3 μC for 6 days [14]. Therefore, the pacemaker must be periodically recharged over the device lifetime, which is intended to be from 1 to 3 months. The pregnant patient would return to the clinic twice a week for follow up and recharging of the micropacemaker until the fetus is delivered. The Quallion Zero-Volt lithium technology can be discharged completely and then recharged without loss of function. This feature improves safety over other lithium cell technology that does not operate according to specification if the cell is fully drained. The micropacemaker will recharge reliably in situations where a recharging session is missed after implantation or drained devices in storage must be charged up quickly for an emergency implantation.

Electromagnetic induction, a mature wireless power methodology used in biomedical applications, can be used to transmit energy to the fetal micropacemaker through the maternal abdomen, recharging the lithium cell. This method relies on inductive coupling between a primary and secondary coil, but is complicated in this application due to the highly variable and random changes in distance and orientation between the coils as a result of fetal movement in the uterus. The shape and size of the secondary coil are severely constrained by the implant form factor and packaging while the size and orientation of the primary coil are constrained by the anatomy of the mother.

Author Manuscript Author Manuscript Author Manuscript Author Manuscript

This paper describes the design of the recharging system while addressing the design constraints that are inherent in a fetal micropacemaker system, and then details the verification of that system.

II. Design

A. Electromagnetic Field Generation

The inductive coupling is expected to be very poor due to a large distance between coils and a very small secondary coil. In air and with ideal alignment, the coupling factor was simulated with a MathCad analysis to be about 0.0005 at physiologically relevant distances (~10cm). Thus the implant needs to optimize magnetic permeability, coil diameter, number of turns and operating frequency in order to generate as much electromotive force (EMF) as possible. The diameter of the secondary coil (2.75 mm) is constrained by the dimension of the surgical tool that drives the diameter of the device. By simultaneously solving for quality factor (Q) of the implant resonant circuit (L_{TANK} and C_{TANK}, Fig. 2) and induced EMF, 23 turns of 3 mil wire was found to generate sufficient current in the implant while not limiting the bandwidth of the device. An operating frequency of 6.78 MHz was chosen because it is high enough to allow an appreciable amount of inductance without too many turns, is low enough to be efficiently generated with modern timing circuits, and is at an unlicensed industrial, scientific and medical (ISM) radio band. To further increase permeability and therefore induced EMF, the secondary coil is wound around a ferrite core made of material 61. Through several design iterations we found that increasing the length of the ferrite core within the package improves recharge current and reduces misalignment effects, but this strategy is limited by the constraint that the entire pacemaker reside completely within the fetal chest.

To multiply the voltage across the load (primarily the rechargeable lithium cell), a parallel resonant circuit topology is used (L_{TANK} and C_{TANK}, Fig. 2); a resonator Q of about 4–6 allows for operation without precise tuning and yet provides the sought after voltage amplification. A half wave rectifier (D_1) maintains a higher equivalent RMS impedance so that the inductance of the implant coil can be allowed to be larger and maintain the Q, while also providing a minimum component count. The RMS equivalent load is half of the DC resistance, neglecting the rectifier diode drop voltage. The lithium cell would require a 4.2 VDC output from the coupling elements and 1.5 mA of current (C/2 recharging speed); this results in a DC resistance of 2800 Ω, and an AC RMS load of 1400 Ω. An inductor in parallel configuration would need a reactance of 350 Ω to maintain a Q of 5.5. This corresponds to an inductance of 8.22 μH. The necessary open circuit EMF of the implant coil would be 4.2 V/5.5 = 0.76 V.

To determine the required electromagnetic field to generate the necessary (MF, we use Faraday's Law of Induction. The changing magnetic field induces an electromotive force, ε, in the implant according to:

$$\varepsilon = -N_2 \, \mu_e \, \tfrac{d}{dt} \, (B \cdot S) \, \text{Volts} \quad (2)$$

Author Manuscript Author Manuscript Author Manuscript Author Manuscript

where N_2 is the number of turns of the secondary coil, μ_e is the effective permeability multiplier, B is the magnetic field density, and S is the surface area of the implant through which the flux is passing. The surface area S is calculated as:

$$S = \pi * r^2 \text{ meters} \quad (3)$$

where r is the radius of the secondary coil. By the Biot-Savart law, a simplification of the magnetic field on axis of a current loop with a number N_1 of current loops on the primary coil is:

$$B = N_1 * \frac{\mu_o R^2 I \sin(\omega t)}{2 (z^2 + R^2)^{\frac{3}{2}}} \text{Teslas} \quad (4)$$

where μ_o is the permeability of free space, R is the radius of the primary coil, I is the current in the primary coil, ω is the radian frequency, and z is the distance from the primary coil on axis. Because the current, and therefore the magnetic field, is sinusoidal, the time derivative yields the following:

$$\varepsilon = -N_2 \mu_e \cdot \omega \cdot B \cdot \pi \cdot r^2 \text{ Volts} \quad (5)$$

The frequency, permeability, and secondary coil are constrained at this point in the design. Therefore, in order to generate the required EMF at the required distance of about 10 cm, we can vary current, number of turns in the primary coil, and diameter of the primary coil. It is desirable to keep the number of turns in the primary coil low to minimize dissipative and dielectric losses in the coil turns. An external coil radius of 20 cm yields the best balance of maximum field range combined with minimal coil power dissipation and coil voltage (Fig. 4).

To generate the oscillating current necessary as found above, a Class-E Oscillator was selected for its high theoretical efficiency and tolerance for operating point shifts [15]. An ideal Class-E Oscillator is characterized by voltage and current waveforms that are out of phase, avoiding power dissipation during switching. Power losses are typically 2 fold lower than for a Class-B or -C topology. Our implementation of this oscillator achieved a power efficiency of 91%, compared with the state of the art (80% to >95%) [15–17]. The field generator (Fig. 5) uses a Pierce Gate Oscillator driven by a 6.78 MHz crystal to generate the correct frequency for the narrow ISM band in which it is desired to operate. The oscillator's signal is buffered through a network to generate enough current to drive the N-Channel MOSFET in the Class-E Oscillator. Both the Class-E oscillator and the transmitting coil use resonance to generate efficiently the large peak current (~8A) and resulting magnetic field required to power the weakly coupled implant.

The transmitting antenna uses a balun (L1, L2) to take the unbalanced output of the Class-E Oscillator and create a balanced input to the center tapped resonant coil, effectively dividing the peak voltage across this coil, thus improving its safety. A network of high voltage RF

Author Manuscript Author Manuscript Author Manuscript Author Manuscript

capacitors provides tuning to resonate the antenna coil and to create a 50 Ω input impedance to match the above-mentioned source. The antenna coil is realized by two turns of cable shielded with copper foil in a discontinuous pattern, thereby reducing radiation of electrostatic fields without generating eddy current loops. As discussed below, a substantial part of the power required to drive this coil reflects dissipative losses arising from eddy currents induced in the conductive tissues of the body. This must be taken into account when designing the impedance matching circuitry in the antenna section.

The MOSFET is configured as a common source amplifier and current is drawn into the drain from a power source through a 5.6 μH RF choke. The power supply voltage can be varied, resulting in the generation of different field strengths, a feature that would become useful if the pacemaker was being recharged too quickly and the field was too strong. This situation could arise if the pacemaker was oriented very favorably and was closer in distance to the primary coil. FCC regulations require the transmitter to generate an electric field strength less than 15 μV/m at 30 m distance from the antenna at the chosen ISM band of 6.78 Mhz. Regulations regarding specific absorption rate (SAR) of human tissue specify that the SAR may not exceed 1.6 W/kg. Including an insulation layer around the antenna ensures that tissue is not in the vicinity of the highest electric field strengths generated, therefore SAR never exceeds this value.

B. Accounting for Non-Ideal Circuit Behaviors

Although solving for generation of current in a load through inductive power analytically yields a logical starting point, the above equations are ideal generalizations. The most problematic assumptions made in the previous analysis include: (1) that the primary and secondary coils are coaligned; (2) that power is transmitted through air; and (3) that the quality factor of the resonant implant is steady in the face of recharging.

Any alignment of primary and secondary coils is plausible in the clinical scenario. The pacemaker, implanted in the fetal chest, will move in all directions with the fetus. Ultrasound imaging will be taken to determine the orientation of the secondary coil before recharging is attempted. Thus, an effort can be made to align the primary coil on the outside of the maternal abdomen with the secondary. The high magnetic permeability of the ferrite core provides a preferred path for local magnetic flux, reducing the effects of small misalignments on coupling, but misalignments greater than about 30° will result in a steep drop in coupling that may limit the rate or final voltage of recharging. If the recharging current is quite low, the operator can be advised to try to reposition the primary coil on the abdomen.

A strong electromagnetic field will generate eddy currents in a nearby conductive plane. The pacemaker will be located within a large amniotic sac encapsulated in less conductive fat and epidermal tissue. The eddy currents that form in these tissues depend on their conductivity and geometry and will oppose the original field, reducing the effective field that the implant sees. The eddy currents formed within those structures are hard to model and are always changing during pregnancy, so various empirical measurements of the reduction in EM field are presented in Section IV.

Author Manuscript Author Manuscript Author Manuscript Author Manuscript

Once current is inductively generated in the implant's secondary coil, current does not flow in the branch of the lithium cell from the half wave rectifier until the voltage built up on the resonant network rises above the voltage of the cell. Q will be high as long as the rectifier is not triggered, and will closely match the ideal conditions calculated above. However, once the voltage across the resonant network builds to a level where current can flow through the rectifying diode, the load of the lithium cell appears to be much larger and Q drops in the circuit. An attempt can be made to increase Q by decreasing the inductance (removing windings on the secondary coil), but this can cause an impedance mismatch between the lithium cell and the resonant network, which can also contribute to less current flowing through the branch to charge the cell. Empirical measurements with a pacemaker simulator circuit in an inductive field reveal the best number of turns to optimize recharge current and are presented in the results.

C. Recharging Control Scheme

Due to the small size of the implant and limited space for regulatory circuitry, the recharging system must be regulated without adding too many components. Incorporating a zener diode for protecting the lithium cell from overcharging was considered, but not ultimately used because of the substantial leakage current associated with the component in the reverse biased condition [18]. Therefore, the strategy employed uses only external monitoring to regulate the recharging process. The pacing rate provides a measure of the voltage supplied by the pacemaker's lithium cell at any time after calibration, which can be used to determine the state of charge of the cell from the discharge profile. The changes in output rate are subtle and actual rates depend on component values that are somewhat variable, so a precise calibration curve of output rate vs. supply voltage is created during the manufacturing of each device (Fig. 3).

Rate is measured *in vitro*, during fabrication and testing, by a simple benchtop system and LabView (National Instruments, 2013) that clocks the interval between each stimulus. Rate is measured *in vivo* by sensing the conducted pacing artifact via skin electrodes placed on the maternal abdomen. The signals are acquired and transmitted to a PC by the BioRadio Wireless Physiological Monitor (Great Lakes Neurotechnologies, Model 150) and analyzed with the same LabView software used for the *in vitro* measurements (Fig. 6).

The state of charge inferred from the calibration curve is used to determine when the pacemaker needs to be recharged and when the pacemaker is fully charged. Overcharging is prevented by manually disabling the inductive field when full charge is detected. It is also important to limit the charging current to prevent damaging the lithium cell. The current varies depending on the strength of coupling between the primary and secondary RF coils. The maximal recharge current produced by the present field generator is typically less than the maximum specified by the manufacturer.

In a more powerful design iteration of the field generator or with an ideal pacemaker position, current may exceed the datasheet limits. In this case, it is useful to measure charging current. This can be done *in vivo* by observing potential developed across any resistance in series with the cell according to E = IR. A series resistor R_B (Fig. 2) was added to the circuit for this reason. For example, a 3 V lithium cell with a combined internal

Author Manuscript Author Manuscript Author Manuscript Author Manuscript

resistance and series resistance of 1 kΩ that is being recharged with 1 mA of current will actually generate 4 V across the relaxation oscillator, causing the oscillator to cycle more quickly. By accurately measuring the output pulse rate when the recharging field is turned on and again when it is turned off, this voltage change and the actual charging current can be computed. If that recharge current is excessive for the ratings of the cell, then the field strength produced by the external transmitter can be reduced manually or programmatically until the rate change is consistent with the desired recharging current. If the recharging current is quite low, the operator can be advised to try to reposition the primary coil on the abdomen.

The charging current calculation can sometimes be unreliable because the intense EM field also causes some changes in rate simply by adding noise to the electronic circuit, confounding the relationship between cell voltage and pacing rate. Therefore, another method is used to calculate current by measuring the change in lithium cell state of charge over time: state of charge is assessed, the EM field and recharging current is applied for a set amount of time and then turned off, and state of charge is measured once again. The difference in state of charge is divided by the amount of time of the recharge, and thus the current is derived. Sudden changes in pacing rate during charging caused by fetal motion can still be detected and used to trigger corrective actions.

D. Calibration

The pacemaker must be meticulously calibrated in order to keep track of the relationship between the supply voltage and the pacing rate. Each device is calibrated initially by varying an external DC supply voltage and measuring the pacing rate at room temperature with a simulated tissue load, a 1 kΩ resistor. Several factors affect this calibration in addition to cell voltage, including the temperature of the device, output impedance, light, electrical noise (especially from the high frequency recharging coil), and recharging current.

To simplify consideration of the factors, we consider here only temperature and output impedance. The factors of light, electrical noise, and current can be eliminated; the pacemaker can be shielded from light and noise during calibration, and current is not present without the recharging field. Temperature and output impedance are the main factors that change immediately upon implantation of the device, because body temperature is about 37 °C and the electrode-tissue interface is comprised of both resistive and capacitive elements. Both temperature and the addition of a capacitive element raise the output rate with respect to supply voltage. The capacitance of the electrodes (the myocardial pacing electrode and reference electrode provided by the lithium cell case) are relatively large but are in series with the output capacitance of the relaxation oscillator, causing the oscillator to see a small reduction in capacitance and therefore a speeding up of pacing rate.

III. Methods

To verify that the recharging system design meets requirements for accurately determining supply voltage and effectively recharging the lithium cell, a combination of *in vitro* and *in vivo* tests were completed. These tests measured the magnetic field generated with the recharging system and the current generated in the implant *in vitro*, assessed the

Author Manuscript Author Manuscript Author Manuscript Author Manuscript

environmental effects on calibration *in vitro* and *in vivo*, and evaluated the performance of the recharging system *in vivo*.

The magnetic field generated with the recharging system was mapped by measuring the signal coupled into a custom made loop probe fashioned out of two turns of AWG 18 copper magnet wire and calibrated based on a known magnetic field. Multiple saline bath configurations (Fig. 8) were used to simulate the conduction of electrical signals through the body and the loading effect that the body has on the primary coil. The range of salinities of the baths was chosen to cover a wider than physiological range of salt concentrations, from 0.34% saline to 5.8% saline, in an attempt to account for different tissue conductivities while also keeping an overall constant load on the primary coil (the primary coil is optimally tuned for the resistive losses seen by a nearby conductor). As the saline configuration was changed, the tuning of the primary coil was also changed to match the effect of the impedance change of the saline.

To determine the current induced in the lithium cell, the field strength was held constant and an ammeter (Agilent 34410A) was added to the pacemaker circuit between elements R_B and the cell. A twisted pair was used in order to minimize the effect of the added circuit element on the system in the large electromagnetic field. The number and spacing of turns of the secondary coil were varied to determine the optimal configuration for generating charging current.

To assess the effects of temperature and impedance on the pacemaker calibration *in vitro*, a pacemaker was subjected to various environments and pacing rate was measured. Temperature was at room temperature (23 °C) or in an oven at body temperature (37–40 °C). The *in vitro* conditions included the comEination of a simulated tissue load, either a 1 kΩ resistor or 0.9% phosphate buffered saline (PBS). A pacing artifact was observed across the simulated tissue load using an amplification circuit or the biopotential recording system (BioRadio 150, Great Lakes NeuroTechnologies) with silver chloride electrodes placed at the surface of the saline. The detected artifact signal was digitized, captured on PC, filtered to eliminate DC drift and high frequencies (LPF=400 Hz, HPF=5 Hz), and the period of the stimulus artifact was measured.

The effect of temperature and impedance on calibration was assessed *in vivo* by observing pacing artifacts over several days during animal studies. The *in vivo* study protocol conformed to the Guide for the Care and Use of Laboratory Animals and was approved by the Institutional Animal Care and Use Committees at the University of Southern California and the Los Angeles Biomedical Research Institute. Fetal micropacemakers with rates between 100 bpm and 150 bpm were implanted into seven fetal sheep according to the procedure discussed in Bar-Cohen, et al. [19]. Devices were implanted fully charged, but supply voltage, and therefore pacing rate, decreased over time, providing observations of pacing rate at different voltages. The fetus was instrumented for these experiments, allowing for detection of the fetal micropacemaker artifact by three transuterine electrodes attached directly to the fetal skin. The percutaneous leads extended out of a maternal abdominal incision and into a pouch sewn on the maternal skin surface for interfacing with the above mentioned biopotential recording system for analysis.

Author Manuscript Author Manuscript Author Manuscript Author Manuscript

The performance of the recharging *in vivo* was assessed by quantifying the shifts in pulse rate described above. After implantation of the pacemaker and during follow up days, recharging was attempted at the discretion of the animal follow up team on sheep 4 – 7. Ultrasound imaging was performed to determine the location and orientation of the pacemaker. The primary coil was placed on or around the maternal sheep to minimize the distance and angle between the primary and secondary coil. Increases in pacing rate during field generation provided a measure of the coupling between the two coils and was used to position the primary coil. The value of resistor R_B was increased in the latter implants (sheep 5, 6, and 7) to improve the sensitivity of this measure.

IV. Results

A. Electromagnetic Field

The magnetic field measured in air with a single homogeneous PBS tissue model [Fig. 7(b) and (c)] matched well with calculated theoretical values. As larger, composite conductive loads were introduced to the field, eddy currents within the load were observed to have a dampening effect on the measured field on the loop probe (Fig. 8). For instance, when comparing normalized magnetic field measured in air at 9– 10 cm [Fig. 8(a)] vs. field measured in any saline load at 9 – 10 cm [Fig. 8(b)–(h)], at least a 48% loss is observed in the best case scenario [Fig. 8(d)].

When comparing composite loads of different configurations, the cross sectional area of each chamber, the conductivity of the solution, and the relative placements were important parameters. A large circular cross sectional area unobstructed by a second compartment, like that in the outer chamber in Fig. 8(b), more greatly attenuated the magnetic field than the smaller cross section in setup Fig. 8(d). The effect of the highly concentrated inner compartment has less of a field cancelation effect when it is further from the plane of the primary coil [Fig. 8(b) vs. Fig. 8(c)]. When comparing similar geometry with hypertonic inner chamber vs outer chamber, the setup with the higher outer chamber concentration [Fig. 8: (h) vs. (d), or (f) vs. (c)] is more greatly attenuated, but this effect is subtle.

B. Current Generation

Current induced in the implant in air [setup shown in Fig. 7(a)] was measured by keeping the device at the optimal location with field strength 30 A/m [centered in the plane of the primary coil, Fig. 9(b)] and at various distances centered above the plane of the primary coil [Fig. 9(c)]. There is a fairly sharp maximum around 18 turns for generating current into the lithium cell when already charged to 3VDC. Comparisons of charging current without the cell voltage in the circuit [Fig. 9(d)] suggest that recharge current is a result of the difference between the available voltage from the resonant circuit and the in-series voltage of the cell. As the number of turns decreases and EMF is reduced, the voltage from the tank circuit spends more and more time below the in-series voltage, thus D_1 spends more time in a non-conductive state. This decrease in recharge current with a reduction in turns is steeper than the case when the in-series voltage is zero and D_1 is conducting a much greater percentage of the time. It was observed that recharge current depended on the polarity (orientation) of the primary coil. This is probably an artifact caused by capacitive coupling between the

Author Manuscript Author Manuscript Author Manuscript Author Manuscript

external primary coil and the implant secondary, which would normally be floating with respect to the RF field generator but which becomes grounded on one end when connected to the current monitoring circuitry. Depending on which way the implant coil was oriented relative to the primary (clockwise or counterclockwise), the capacitive coupling between the primary and secondary coils either added to or subtracted from the signal generated on the resonant network of the implant recharging circuitry, resulting in either an overestimate or an underestimate of the recharging current, respectively. In Fig. 9, as expected, the distance of the + and – polarity traces from the mean increases with number of turns, corresponding with an increase in capacitance between the primary and secondary coils. The 4 mA recharge current at the strongest point in the field in air will be somewhat attenuated in tissue, estimated to reach about 2 mA at the plane of the coil and 1 mA at 10 cm away.

C. Calibration In Vitro

The pacemaker used in sheep study 7 was analyzed *in vitro* and demonstrated variations in pacing rate due to temperature and impedance changes. The pacing rate increased with a nearly linear offset by an average of 3.4 bpm from temperature alone, 9.2 bpm from electrode capacitance in PBS alone, and 11.0 bpm from the combined effects of temperature and interface capacitance together (Fig. 10).

D. Calibration and Recharging In Vivo

Although the fetal sheep model presented some unique challenges for implantation compared to a hydropic human fetus, calibration and recharging was able to be assessed on a subgroup of the total sheep implanted. Detailed results regarding the micropacemaker efficacy for each sheep can be found in Bar-Cohen et al. [19]. The first 3 sheep studies were focused on device implantation and successful pacing capture; calibration data recording and recharging experiments were done in sheep 4, 5, 6, and 7.

1) Calibration In Vivo—When the pacemaker was implanted into sheep 7 on operational day (OD), an initial offset of 10.6 bpm was observed (Fig. 11), similar to the offset observed *in vitro* in 39 °C PBS. On post operational day 2 (POD2) the pacing rate was observed to have a new offset of 12.9 bpm. The measured increase of pacing rate offset from OD to POD2 indicates that the effective capacitance of the oscillator circuit was decreasing. This means that the capacitance at the frequencies of interest of the electrode-tissue interface was decreasing, perhaps related to the change in the electrode-tissue interface as various biochemical and cellular components of the foreign body reaction were deposited. This is consistent with data in the literature that show increasing impedances at low frequencies, a reflection of decreasing interface capacitance [20]. Quantifying the exact changes to the impedance of the system is out of the scope of this manuscript. However, based on our observations *in vivo*, these changes seem to stabilize sufficiently within 2 days after implantation to assume an overall capacitance change, and to select an offset value for the calibration.

Four different implanted pacemakers generated data regarding the pacing rate offset over time. The original calibration curve (dotted line, Fig. 11) was fitted with a two term exponential function and then linearly shifted by a factor proportional to the relative pacing

Author Manuscript Author Manuscript Author Manuscript Author Manuscript

rate, as each device has a slightly different rate based on actual component values. The offset calibration curve (solid line, Fig. 11) agreed well with the pacing rate predicted from lithium cell depletion as a result of pacing current draw for 1–3 post-operative days (PODn, Fig. 11; discrete data points, o).

2) Recharging—Recharging efforts in sheep 4 were not successful and did not result in any observed change in state of the lithium cell. It was later determined that the recharging system hardware had some tuning and heating malfunctions, which were resolved by replacement of components, retuning, and long duration burn-in tests.

In sheep 5, pacing capture was not successful when a first device was implanted. A second device was then advanced and anchored, resulting in successful pacing capture of both devices. Recharging efforts on POD12 were successful at waking up both implants after they had been completely depleted. The two devices were nearly side by side, and recharged to about the same level. Device I recharged to 2.6 V and Device II recharged to 2.8 V.

The device implanted into sheep 6 was able to be recharged to between 3.0 to 3.4 V on POD2. Recharging was performed for just a short time in sheep 7, but changes in pacing rate were observed. Low speeds of charging (current) were observed in all recharging attempts. These implants were built with ferrites that were 6 mm long; the results in Fig. 9 were obtained with devices that used 9 mm long ferrites, which produced about twice the recharge current for comparable charging configurations.

V. Discussion

The recharging system demonstrated here successfully generated the expected electromagnetic field. Realized currents *in vitro* were adequate for recharging, but *in vivo* currents were lower than calculations predicted due to several reasons. Eddy currents generated within the conductive media surrounding the implant attenuate the field that reaches the secondary coil. Due to the iterative process of device development, the implants used in *in vivo* experiments had high R_B values, smaller ferrites, and were not tuned perfectly to the desired resonant frequency. The higher R_B values limit the amount of current generated into the implant and was reduced in subsequent devices to increase charging current, at the expense of a less sensitive indicator of recharge current. These three shortcomings were corrected and the data presented in Fig. 9 was obtained from optimized devices.

Increasing field strength would improve current generated in the implant and could be done by increasing the number of turns on the primary coil and/or increasing current in the primary coil. Both of these would lead to higher peak voltages in the primary coil and would require components with higher power and voltage ratings.

The linear offset of the calibration to accommodate environmental effects fits the data on the limited implants tested for the limited durations tested. Further *in vivo* tests to ensure that the proposed calibration shifts are stable would be useful for validation of this approach. Future work will involve incorporating environmental factors that were not considered here,

Author Manuscript Author Manuscript Author Manuscript Author Manuscript

such as light, electrical noise, and a greater sample of temperatures and impedances, leading to the formation of a multivariable calibration equation.

Results from the *in vivo* recharging efforts were promising, although more studies are required to demonstrate repeated recharging *in vivo*. The current work was restricted due to limited time available for follow-up with the subjects and difficulties aligning the primary and secondary coils, largely due to anatomy of the pregnant ewes and poor imaging quality that hampered the ability to locate implants before recharging. Current in devices was induced *in vivo*, as evidenced by the change in voltage over time of the pacemakers, however, this current was less than expected. Changes in device design to amplify the induced current were completed after animal studies had concluded, so the *in vivo* studies were not able to take advantage of these improvements. Time was limited during follow up visits because of animal handling restrictions.

Recharging in the clinical setting will have several advantages that were not available during pre-clinical studies so far. The anatomy of human pregnancy mid-gestation provides superior ultrasound conditions to the sheep anatomy observed in this study. Image quality in a human fetus is expected to be much clearer, improving the ability of the clinical team to locate the micropacemaker and align the coils for recharging. The latest pacemaker design iteration with a longer ferrite will provide better coupling, the pregnant mother will be responsive to direction, and recharging time can be extended to deal with poor orientations, which may improve as the fetus repositions itself in the uterus.

Current state-of-the-art inductive power systems have not demonstrated successful recharging of an implant battery with the environment, dimensions, and specifications similar to the ones demonstrated here. Currently available pacemaker systems do not incorporate wireless recharging, most likely because their relatively large size accommodates modern primary cells that enable pacemaker lifetimes of over 10 years and they use titanium hermetic packages that would interfere with wireless power transmission. Future iterations of the micropacemaker could improve battery life and functionality further by utilizing integrated circuit technologies. This would probably require a hermetic package to protect the more sensitive circuitry from moisture over longer periods of time. Such packaging remains challenging at the dimensions of the fetal micropacemaker.

VI. Conclusion

Our transcutaneous RF recharging system successfully transmits adequate power to a fetal micropacemaker, overcoming challenges in packaging constraints and fetal anatomy. As demonstrated by the *in vitro* and *in vivo* testing, current is generated in the device and recharging can be monitored to ensure a full recharge and patient safety. To the best of our knowledge, this is the first demonstration of successful wireless power with a non-stationary secondary coil implanted in a fetus. The rotating fetus and attenuation of electromagnetic field in the highly conductive amniotic fluid decrease the efficiency of the wireless power transfer, but a well-tuned implant with a ferrite that maximizes permeability yields the best chance for a full recharge. Further testing will continue to optimize the recharging of our device for future clinical studies.

Author Manuscript Author Manuscript Author Manuscript Author Manuscript

This work is a positive proof of concept that wireless power is feasible in deeply implanted devices, and the findings could be instrumental for future designs of micropacemakers or other stimulators that are to be implanted deep within tissue.

Acknowledgments

This work was supported by the Coulter Foundation, the Wright Foundation, the Southern California Clinical and Translational Science Initiative, and the National Institutes of Health under Grant 5R01HD075135-02.

The authors would like to thank Drs. Michael Silka, Jay Pruetz, and Catalina Guerra for assistance in imaging, implanting devices, and clinical expertise; consultant Ray Peck for fabrication and engineering expertise; and engineers Kaihui Zheng, Michael Lu, Hithesh Reddivari, Shane Garcia, and Michael Maylahn for contributions to hardware, software, and animal study preparation.

References

1. Friedman DM, Kim MY, Copel JA, Davis C, Phoon CKL, Glickstein JS, et al. Utility of Cardiac Monitoring in Fetuses at Risk for Congenital Heart Block. Circulation. 2008; 117:485–493. [PubMed: 18195175]
2. Lopes LM, Tavares GMP, Damiano AP, Lopes MAB, Aiello VD, Schultz R, et al. Perinatal Outcome of Fetal Atrioventricular Block. Circulation. 2008; 118:1268–1275. [PubMed: 18765396]
3. Groves AM, Allan LD, Rosenthal E. Outcome of isolated congenital complete heart block diagnosed in utero. Heart. 1996; 75:190–194. [PubMed: 8673760]
4. Schmidt KG, Ulmer HE, Silverman NH, Kleinman CS, Copel JA. Perinatal outcome of fetal complete atrioventricular block: A multicenter experience. Journal of the American College of Cardiology. 1991; 17:1360–1366. [PubMed: 2016455]
5. Ho A, Gordon P, Rosenthal E, Simpson J, Miller O, Sharland G. Isolated Complete Heart Block in the Fetus. The American journal of Cardiology. 2015
6. Carpenter RJ Jr, Strasburger JF, Garson A Jr, Smith RT, Deter RL, Tristan Engelhardt H Jr. Fetal ventricular pacing for hydrops secondary to complete atrioventricular block. Journal of the American College of Cardiology. 1986; 8:1434–1436. [PubMed: 3782646]
7. Silverman, NH., Kohl, T., Harrison, MR., Hanley, FL. Experimental fetal surgery in the animal model and in the human fetus. Second World Congress of Pediatric Cardiology and Cardiac Surgery; Honolulu, HI. 1998. p. 622-3.
8. Eghtesady MEP, Knilans TK, Witte DP, Manning PB, Crombleholme TM. Fetal surgical management of congenital heart block in a hydropic fetus: lessons learned from a clinical experience. J Thorac Cardiovasc Surg. 2011:835–7. [PubMed: 20674938]
9. Walkinshaw SA, Welch CR, McCormack J, Walsh K. In utero Pacing for Fetal Congenital Heart Block. Fetal Diagnosis and Therapy. 1994; 9:183–185. [PubMed: 8060513]
10. Assad RS, Zielinsky P, Kalil R, Lima G, Aramayo A, Santos A, et al. New lead for in utero pacing for fetal congenital heart block. The Journal of Thoracic and Cardiovascular Surgery. 2003; 126:300–302. [PubMed: 12878975]
11. Zhou L, Vest AN, Peck RA, Sredl JP, Huang X, Bar-Cohen Y, et al. Minimally Invasive Fetal Micropacemaker: Mechanical Testing and Refinements. Medical & Biological Engineering & Computing. 2016
12. Bernstein AD, DAUBERT JC, FLETCHER RD, HAYES DL, LüDERITZ B, REYNOLDS DW, et al. The Revised NASPE/BPEG Generic Code for Antibradycardia, Adaptive- Rate, and Multisite Pacing. Pacing and clinical electrophysiology. 2002; 25:260–264. [PubMed: 11916002]
13. Vest AN, Zhou L, Bar-Cohen Y, Loeb GE. A novel method to estimate safety factor of capture by a fetal micropacemaker. Physiological Measurement. 2016; 37:1172–1185. [PubMed: 27340134]
14. Nicholson, A., Chmait, RH., Bar-Cohen, Y., Zheng, K., Loeb, GE. Percutaneously injectable fetal pacemaker: electronics, pacing thresholds, and power budget. Annual International Conference of the IEEE Engineering in Medicine and Biology Society; San Diego, CA. 2012.
15. Sokal NO. Class-E RF power amplifiers. QEX Commun Quart. 2001; 204:9–20.

Author Manuscript Author Manuscript Author Manuscript Author Manuscript

16. Ebert J, Kazimierczuk M. Class E High-Efficiency Tuned Power Oscillator. IEEE Journal of Solid-State Circuits. 1981; SC.16:62–66.
17. Kazimierczuk M, Krizhanovski V, Rassokhina J, Chernov D. Class-E MOSFET Tuned Power Oscillator Design Procedure. IEEE Transactions on Circuits and Systems. 2005; 52:1138–1147.
18. Loeb GE, Zhou L, Zheng K, Nicholson A, Peck RA, Krishnan A, et al. Design and testing of a percutaneously implantable fetal pacemaker. Annals of biomedical engineering. 2013; 41:17–27. [PubMed: 22855119]
19. Bar-Cohen Y, Loeb GE, Pruetz JD, Silka MJ, Guerra C, Vest AN, et al. Preclinical Testing and Optimization of a Novel Fetal Micropacemaker. Heart Rhythm. 2015; 12:1683–1690. [PubMed: 25778431]
20. Lempka SF, Miocinovic S, Johnson MD, Vitek JL, McIntyre CC. In vivo impedance spectroscopy of deep brain stimulation electrodes. Journal of neural engineering. 2009; 6:046001. [PubMed: 19494421]

Biographies

Adriana N. Vest received a B.E. degree in Biomedical Engineering from Vanderbilt University, Nashville, TN, in 2009 and the M.S. and Ph.D. degrees in Biomedical Engineering from the University of Southern California, Los Angeles, CA, in 2015.

After completing her doctorate, she joined the Neurological Biomaterials and Cancer Therapeutics Laboratory at Georgia Institute of Technology and the Clifford Lab at Emory University. Her research interests include clinical technology translation, medical devices, instrumentation, and signal processing.

Li Zhou completed his M.S. degree in materials science and his Ph.D. in Biomedical Engineering with a focus on medical device design and development at University of Southern California, Los Angeles, CA in 2016.

He is now an Engineer at Medtronic Diabetes in Northridge, CA.

Author Manuscript Author Manuscript Author Manuscript Author Manuscript

Xuechen Huang received a B.S. degree in Biomedical Engineering from the Southern Medical University, Guangzhou, China, in 2012, and the M.S. degree in Biomedical Engineering from the University of Southern California, Los Angeles, CA, in 2014. He is currently pursuing his Ph.D. degree in Biomedical Engineering at the Viterbi School of Engineering, University of Southern California, Los Angeles, CA.

Since 2013, he has been a Research Assistant with the Medical Device Development Facility. His research interests focus on applied electrophysiology in neural control for muscle strengthening and function rehabilitation. His research and engineering efforts include wireless recharging systems, medical packaging, implantable neuromuscular micro-stimulators, and animal study and clinical trial design.

Mr. Huang was a recipient of the Provost Fellowship from University of Southern California in 2014.

Viktoria Norekyan is pursuing a B.S. in Biomedical Engineering with an electrical emphasis at the University of Southern California, Los Angeles, CA. Her professional interests include medical device design and commercialization.

Yaniv Bar-Cohen is a pediatric electrophysiologist and the Director of Cardiac Rhythm Devices at Children's Hospital Los Angeles. He is an Associate Professor of Pediatrics and Medicine at the Keck School of Medicine at the University of Southern California.

Author Manuscript Author Manuscript Author Manuscript Author Manuscript

Ramen H. Chmait, MD, is Associate Professor of Obstetrics and Gynecology at the University of Southern California, Keck School of Medicine, and Director of Los Angeles Fetal Surgery.

Gerald Eli Loeb (M ’80) M.D. Johns Hopkins, NIH (1973–1988), Prof. Physiology, Queen’s Univ. (1988–1999); now Professor of Biomedical Engineering & Director of the Medical Device Development Facility, University of Southern California, Los Angeles, CA.

Author Manuscript Author Manuscript Author Manuscript Author Manuscript

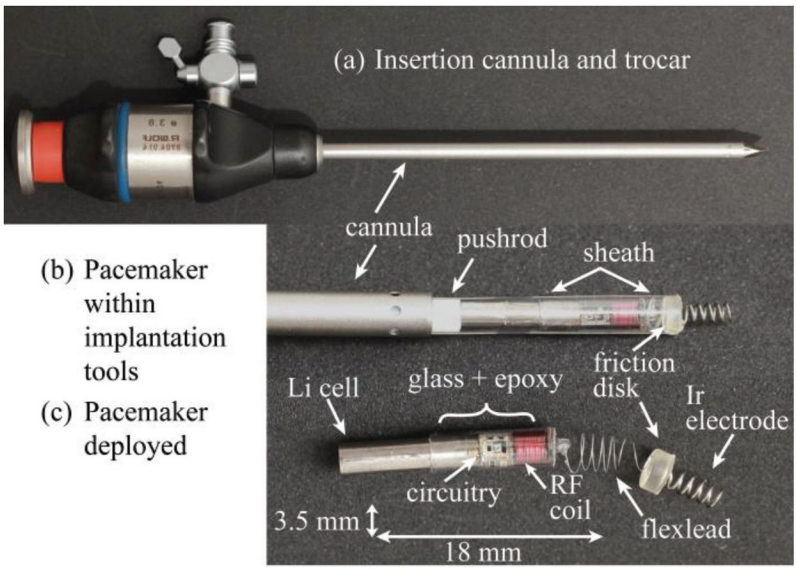

Fig. 1.

Micropacemaker insertion strategy. (a.) Insertion cannula and trocar (b.) Pacemaker before deployment in insertion sheath (c.) Pacemaker after deployment. (From Zhou et al. Permission granted.)

Author Manuscript Author Manuscript Author Manuscript Author Manuscript

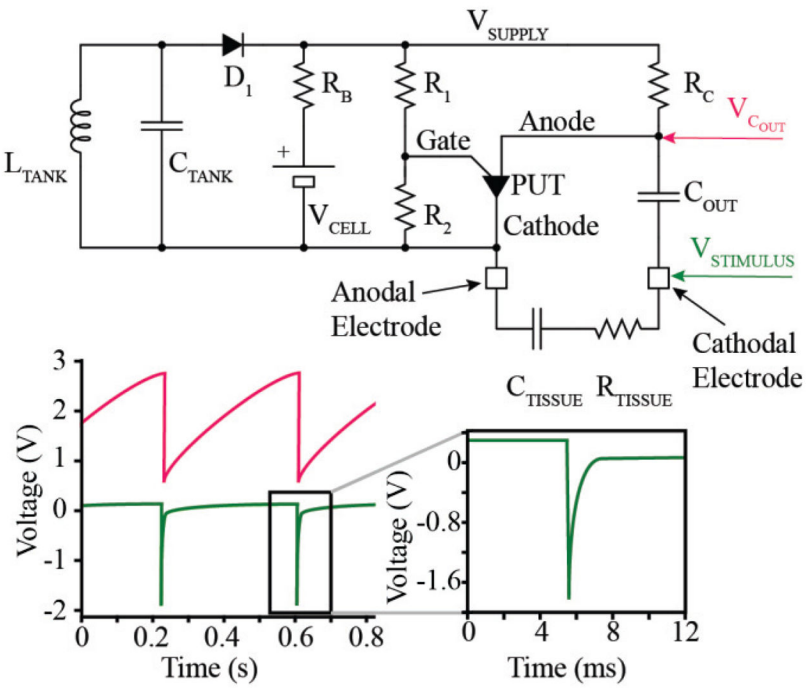

Fig. 2.

Schematic and SPICE simulation of pacemaker. The pacemaker provides an exponential decay pulse utilizing a relaxation oscillator.

Author Manuscript Author Manuscript Author Manuscript Author Manuscript

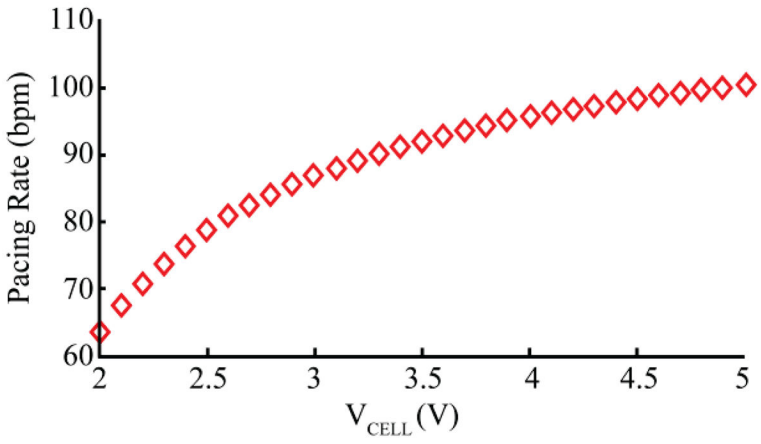

Fig. 3.

Calibration curve. A typical calibration for a pacemaker. Each pacemaker is serialized and then calibrated so that the pacing rate can be used as a measure of cell voltage.

Author Manuscript Author Manuscript Author Manuscript Author Manuscript

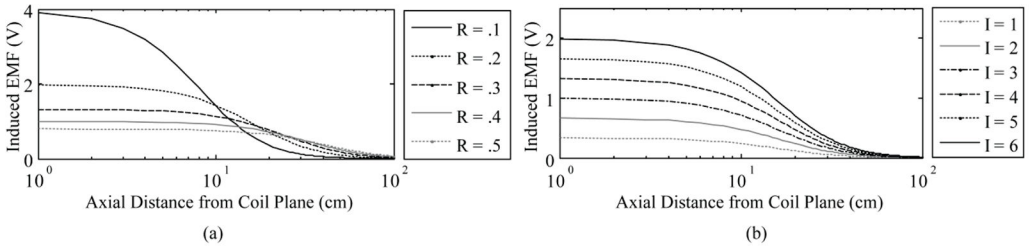

Fig. 4.

EMF vs. distance from primary coil. Radius (R in meters) is varied (left) and current (I in amperes) is varied (right) of the primary coil to determine the EMF that can be generated in the implant. Values shown are before Q is accounted for.

Author Manuscript Author Manuscript Author Manuscript Author Manuscript

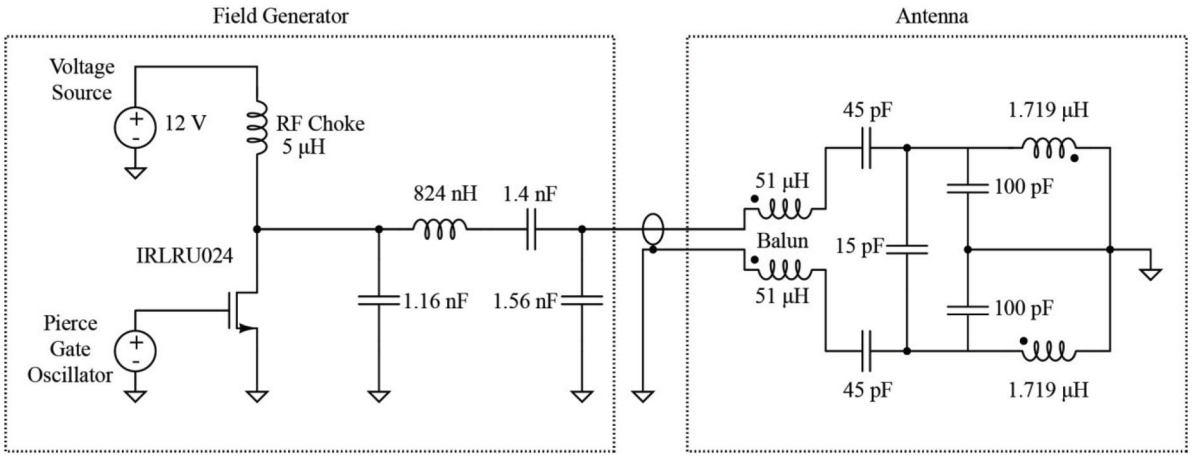

Fig. 5.

Schematic of the coil driver and antenna. A Class E-Oscillator (left) generates the 6.78 MHz sine wave that drives the Antenna (right).

Author Manuscript Author Manuscript Author Manuscript Author Manuscript

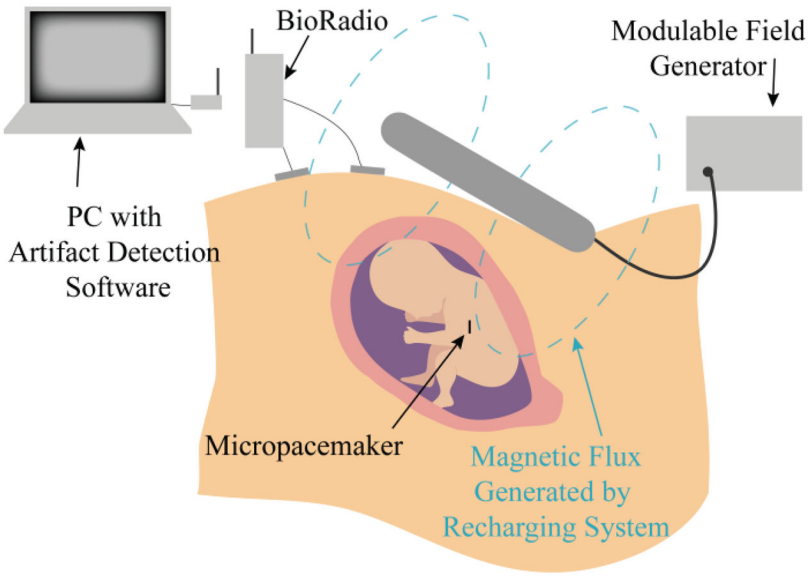

Fig. 6.

Diagram of the recharging strategy. The artifact detection system monitors the pacing rate of the pacemaker and infers lithium cell voltage, given a calibration curve associated with each serially numbered device. A modulable field generator can be adjusted if the recharging is determined to be too fast or too slow.

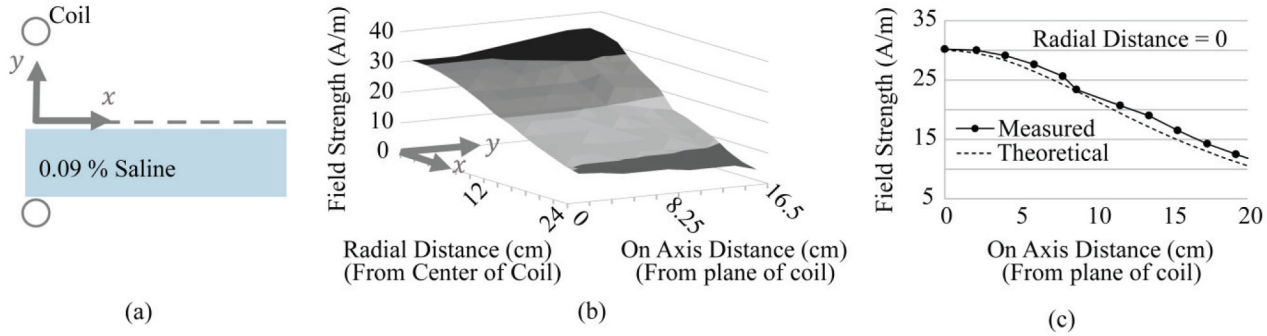

Fig. 7.

Field and current measurements *in vitro*. (a) Measurement setup diagram. (b) The electromagnetic field dropped off with distance from the coil (on axis) and increased with distance from the center (radial). (c) The measured field strength at the center of the primary coil and as distance increased from the plane of the coil (on axis) matched the theoretical calculation.

Author Manuscript Author Manuscript Author Manuscript Author Manuscript

Author Manuscript Author Manuscript Author Manuscript Author Manuscript

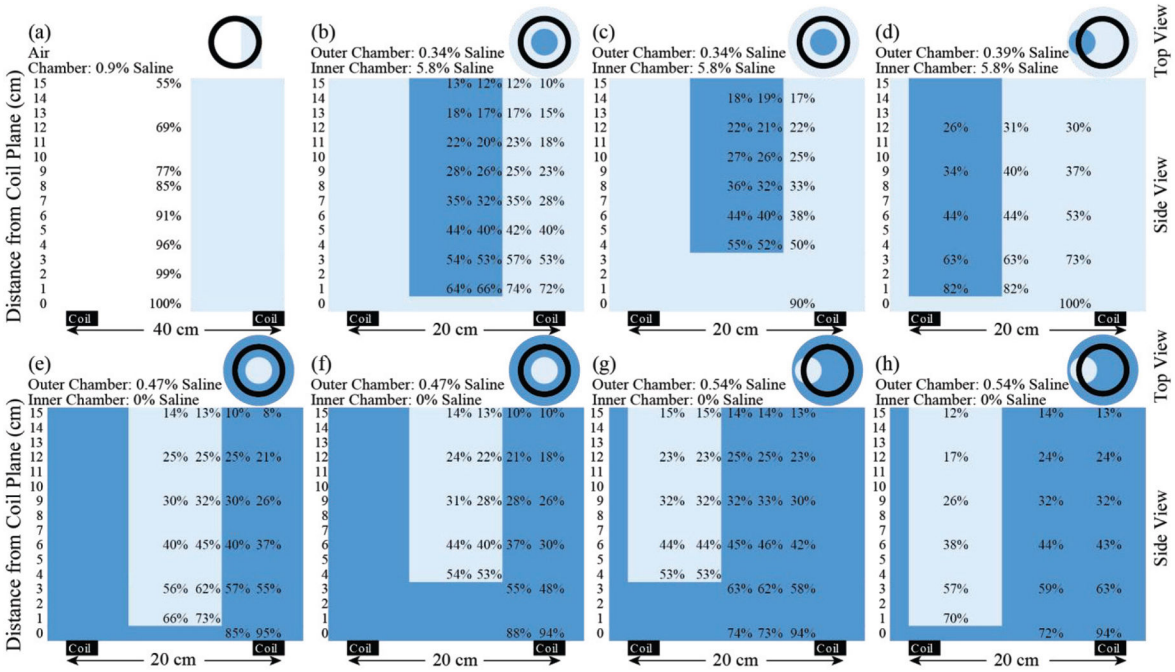

Fig. 8.

Normalized magnetic field detected with a loop probe in various conductive environments. Magnetic field was normalized to the peak field detected in each bath setup. Light blue represents the solution with the lower concentration for the given bath setup, while dark blue represents the higher concentration solution.

Author Manuscript Author Manuscript Author Manuscript Author Manuscript

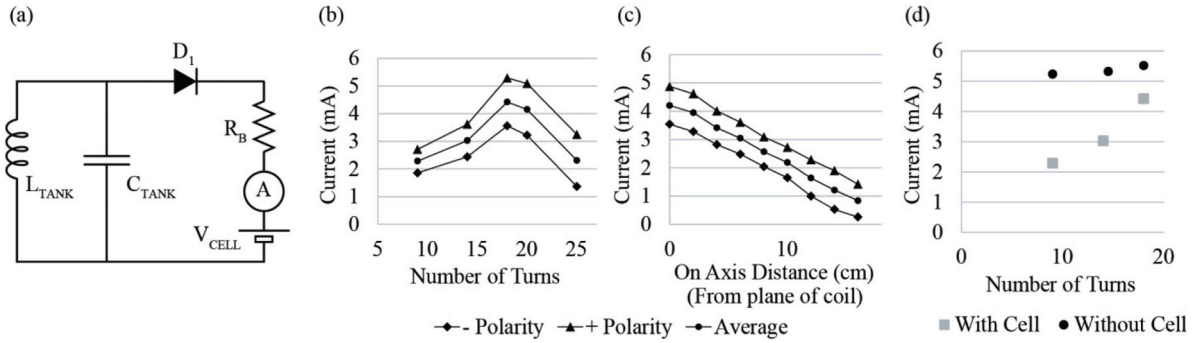

Fig. 9.

Induced implant current *in vitro*. (a) Schematic for current detection circuit. (b) Optimization of induced current by the number of turns. (c) Current detected on 18 turn coil as a function of increasing distance away from the plane of the coil. (d) Current induced in the implant with and without the lithium cell.

Author Manuscript Author Manuscript Author Manuscript Author Manuscript

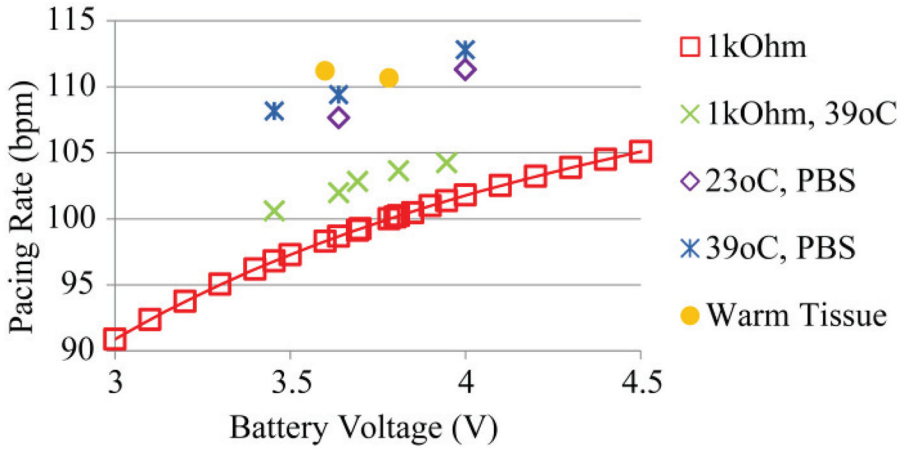

Fig. 10.

Effects on calibration. A pacemaker originally calibrated (red squares) is subjected to various environments to determine the effects on the calibration curve. The effects of the body (yellow filled in circles) cannot be completely simulated in a warm saline bath (blue stars).

Author Manuscript Author Manuscript Author Manuscript Author Manuscript

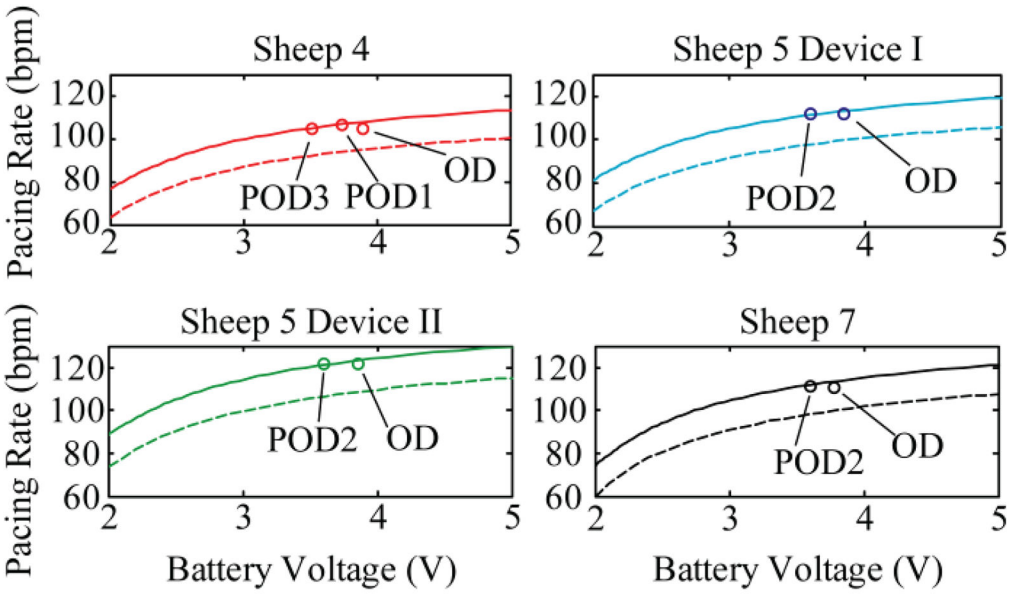

Fig. 11.

Corrected calibration curves. Calibrations (dotted lines) for different devices were linearly shifted (solid lines) to predict a new calibration for an *in vivo* environment. Data points taken during *in vivo* testing are plotted (circles), indicating the quality of the prediction. Full effect of the *in vivo* scenario was not complete on the first day (operational day, OD), hence the offset of the actual value from the prediction.